



SCIENTIFIC REPORTS



OPEN

Fluorescence correlation spectroscopy reveals a cooperative unfolding of monomeric amyloid- β 42 with a low Gibbs free energy

Mario Schneider¹, Stefan Walta², Chris Cadek¹, Walter Richtering ² & Dieter Willbold ^{1,3}

The amyloid-beta peptide ($A\beta$) plays a major role in the progression of Alzheimer's disease. Due to its high toxicity, the 42 amino acid long isoform $A\beta_{42}$ has become of considerable interest. The $A\beta_{42}$ monomer is prone to aggregation down to the nanomolar range which makes conventional structural methods such as NMR or X-ray crystallography infeasible. Conformational information, however, will be helpful to understand the different aggregation pathways reported in the literature and will allow to identify potential conditions that favour aggregation-incompetent conformations. In this study, we applied fluorescence correlation spectroscopy (FCS) to investigate the unfolding of Alexa Fluor 488 labelled monomeric $A\beta_{42}$ using guanidine hydrochloride as a denaturant. We show that our $A\beta_{42}$ pre-treatment and the low-nanomolar concentrations, typically used for FCS measurements, strongly favour the presence of monomers. Our results reveal that there is an unfolding/folding behaviour of monomeric $A\beta_{42}$. The existence of a cooperative unfolding curve suggests the presence of structural elements with a Gibbs free energy of unfolding of about 2.8 kcal/mol.

Aggregation of amyloid-beta ($A\beta$) is believed to be one of the key processes in the development and progression of Alzheimer's disease (AD). Monomeric $A\beta$ is formed by cleavage of the amyloid precursor protein (APP) by β - and γ -secretases. Depending on the exact cleavage sites of the secretases, different isoforms of the monomeric $A\beta$ evolve and are released into the extracellular space. The high aggregation propensity of $A\beta_{42}$ even at low micromolar concentrations is a major problem to elucidate the monomer structure in purely aqueous solutions by conventional techniques such as nuclear magnetic resonance (NMR) spectroscopy or X-ray diffraction. Therefore, information about $A\beta_{42}$ monomer conformation exists so far only from solutions containing hexafluoroisopropanol (HFIP)^{1,2}. However, these conditions are far from being physiological, especially because typical $A\beta_{42}$ concentrations *in vivo* are in the nanomolar range³. Thus, there is not much experimental evidence on the structural properties of $A\beta$ monomers. Understanding the structural conversions of $A\beta_{42}$ during aggregation can be the basis for drug development and AD treatment. It is suggested that the $A\beta_{42}$ monomer might exist in equilibrium between a folded and unfolded conformer⁴, but to date there is no substantial experimental evidence for this hypothesis.

In this study, we applied fluorescence correlation spectroscopy (FCS) to follow changes in the hydrodynamic radius of dye-labelled $A\beta_{42}$ and thus to be able to observe its unfolding transition with increasing guanidine hydrochloride (GdnHCl) concentrations. Since FCS measurements are typically performed at low nanomolar concentrations, this technique is well-suited to study dye-labelled $A\beta_{42}$ monomers.

Our findings demonstrate that $A\beta_{42}$ shows a cooperative unfolding pattern when denatured with GdnHCl under near-physiological conditions. The Gibbs free energy of unfolding was determined to be about 2.8 kcal/mol, thereby indicating that stable structural elements are present.

¹Institut für Physikalische Biologie, Heinrich-Heine-University Düsseldorf, Düsseldorf, Germany. ²Institute of Physical Chemistry, RWTH Aachen University, JARA - Soft Matter Science, Aachen, Germany. ³Institute of Complex Systems, Structural Biochemistry (ICS-6), Research Center Jülich, Jülich, Germany. Mario Schneider and Stefan Walta contributed equally to this work. Correspondence and requests for materials should be addressed to D.W. (email: d.willbold@fz-juelich.de)

Materials and Methods

C(0)A β 42 dye labelling and purification. We dissolved lyophilized recombinant A β 42 with an additional cysteine residue at the N-terminal end (position zero) “C(0)A β 42” (preparation is described in the Supplementary Information), in 6 M GdnHCl (pH 7.4) containing a 10-fold molar excess of tris(2-carboxyethyl) phosphin (TCEP). 1 mg of Alexa Fluor 488 maleimide (Molecular Probes, Eugene, OR, USA) was dissolved in 100 μ L DMF (*N,N*-Dimethylformamide Uvasol for spectroscopy, Merck, Darmstadt, Germany) and added to the reaction mixture in order to maintain a 5-fold molar excess of the dye. The labelling reaction at the N-terminal cysteine residue was performed at room temperature overnight. Hereafter, unreacted dye was separated from labelled C(0)A β 42 (termed AF488-C(0)A β 42) by reversed-phase high performance liquid chromatography (rp-HPLC) with 29% Acetonitrile/H₂O + 0.1% TFA and at 80 °C. Furthermore, the resulting dye-conjugate fraction was lyophilized (SpeedVac (AVC 2-18) with cold-trap LT-105, Christ, Osterode am Harz, Germany) and stored at –80 °C until further use.

Our dye-conjugate variant of A β 42 with an additional cysteine at the N-terminus is expected to have the same structural properties as the unmodified A β 42. The insertion of the uncharged amino acid cysteine at the N-terminus, which is known to be unstructured^{4,5}, is not expected to change the properties of our monomer. Compared with the dye molecule, the additional cysteine contributes less molecular weight than the dye itself and acts as a linker between the dye and the A β 42 to prevent interference between the dye and the A β peptide⁶. Based on the most direct and important property of A β 42 we did not find any drastic change. In particular, we found that the dye-conjugate of C(0)A β 42 is able to aggregate exactly as A β 42, as shown in the size exclusion chromatography (SEC) (Fig. S1) of C(0)A β 42 indicating aggregates thereof eluting earlier than the C(0)A β 42 monomers.

Preparation of guanidine hydrochloride solutions. All solutions were prepared with Milli-Q water (Merck Millipore, Darmstadt, Germany) and high-purity 8 M GdnHCl stock solution. The 8 M GdnHCl stock solution was used to prepare a 6 M GdnHCl solution in 125 mM phosphate buffer at pH 7.4. The resulting solution was then further used to prepare GdnHCl solutions ranging from 0 to 6 M in 125 mM phosphate buffer (pH 7.4) for the unfolding experiments. The GdnHCl concentration of each solution was checked by refractive-index measurements (Refractometer, Bausch & Lomb, Rochester, NY, USA) using an empirical relation between GdnHCl concentration and refractive index, as described by Nozaki *et al.*⁷. Additionally, we measured the kinematic viscosity (micro-Ostwald Viscosimeter with capillary type I, LAUDA Dr. R. Wobser GmbH & Co. KG, Lauda-Königshofen, Germany) and the density (Density meter DMA 5000, Anton Paar, Scharnhausen, Germany) of each of these GdnHCl solutions to obtain the dynamic viscosity at 23 °C. This was needed in order to convert the diffusion coefficient into a hydrodynamic radius, as shown in the Supplementary Information.

1-focus fluorescence correlation spectroscopy measurements. 1-focus fluorescence correlation spectroscopy (1fFCS) measurements were performed on a home-built confocal fluorescence detection setup equipped with a pulsed laser diode ($\lambda = 470$ nm, LDH-P-C-470, PicoQuant, Berlin, Germany). The laser light is forwarded into the microscope via a dichroic mirror (dichroic mirror z470/635, AHF Analysentechnik, Tübingen, Germany). A water-immersion objective (UplanApo 60 \times 1.2 W, Olympus, Melville, NY, USA) focuses the laser beam into the sample solution where fluorescent molecules are excited. Fluorescence light is collected by the same objective in reverse direction, passing through the dichroic mirror and focused onto a pinhole of 100 μ m diameter by a tube lens. A polarising beam splitter separates photons according to their polarisation. Each beam is subsequently focused onto a single-photon avalanche detector (SPAD) detector (PDM, MPD, Bolzano, Italy). For fluorescence correlation spectroscopy (FCS) analysis, the signals from both detectors were cross-correlated to remove detector artifacts such as afterpulsing⁸.

FCS measurements were conducted in a 389 well-plate (384 Well Greiner Microplate, Greiner Bio-One, Frickenhausen, Germany) covered with foil to prevent solvent evaporation. The correction collar was adjusted to gain maximum intensity when measuring a concentrated solution (~10 nM) of Alexa Fluor 488 (AF488). A laser power of about 20 μ W was chosen to prevent triplet formation and saturation effects. The concentration of AF488-C(0)A β 42 was about 3 nmol/L. The correlation and the following fitting were performed using custom software written in MATLAB (The MathWorks, Natick, MA, USA). A typical FCS measurement contained more than 20 million detection events. This data was subsequently split into subpackages of 2 million events resulting in 10 correlation curves for each GdnHCl concentration. The correlation curves were fitted by a one-component diffusion model and subsequently converted into hydrodynamic radii by the Stokes-Einstein relation. Further details on data fitting and evaluation can be found in the Supplementary Information.

Dual-focus fluorescence correlation spectroscopy measurements. Dual-focus fluorescence correlation spectroscopy (2fFCS) measurements were performed on a time-resolved confocal fluorescence microscopy system (MicroTime 200 with dual-focus option, PicoQuant, Berlin, Germany). For excitation, two identical laser diode heads ($\lambda = 470$ nm, LDH-P-C-470, PicoQuant, Berlin, Germany) provide synchronised laser pulses with alternating orthogonal polarisation. According to this polarisation, the laser pulses are deflected in two slightly different directions by a Nomarski prism (U-DICTHC, Olympus, Melville, NY, USA), which is placed in front of the water-immersion objective (UPLSAPO 60xW, 1.2 N.A., Olympus, Melville, NY, USA). In this way, two overlapping but laterally shifted foci are generated in the sample. Because the lateral distance remains constant over time for a given wavelength, absolute values of the diffusion coefficient can be measured⁹.

2fFCS measurements were conducted in sealed sample cells at 23 °C, whereas an absolute accuracy of 0.1 °C is achieved by homemade temperature regulation¹⁰. The total laser power was adjusted to approximately 50 μ W, before the laser light is reflected towards the objective. The measurement time was adjusted to detect 4×10^6 photons per point at least. The detected photons were divided into 2×10^6 photon subpackages. Several points were recorded for each sample. The resulting autocorrelation and cross-correlation functions were fitted by a

one-component diffusion model. The obtained diffusion coefficients were averaged over all measured data points and converted into hydrodynamic radii by the Stokes-Einstein relation. Further details on the 2fFCS setup, data fitting and evaluation can be found in the Supplementary Information.

Photon Counting Histogram analysis. Photon counting histogram (PCH) analysis was performed to check if the amyloid beta molecule solely exists in its monomeric form under low-nanomolar concentrations. PCH analysis is a powerful tool to discriminate different molecules based on their brightness. Müller *et al.* demonstrated that PCH is capable of distinguishing singly and doubly labelled proteins¹¹. Thus, PCH is complementary to FCS which is not able to resolve two fluorescent molecules of similar size¹². Additionally, PCH is especially useful when molecules tend to form oligomers¹³. The basics of PCH analysis are briefly described in the Supplementary Information. For more details, we refer to the paper by Chen *et al.*¹⁴.

Unfolding curve data analysis. By plotting the hydrodynamic radius R_H versus the denaturant concentration, an experimental curve was obtained which is referred to as experimental unfolding curve subsequently. A two-state unfolding model was applied to fit the experimental unfolding curves (equation (1)) by using a Levenberg-Marquardt simplex algorithm in Origin (OriginLab, Northampton, MA, USA).

$$R_H = \frac{R_{H,N} + R_{H,U} \exp\left(-\frac{\Delta G^{H_2O} - m [D]}{RT}\right)}{1 + \exp\left(-\frac{\Delta G^{H_2O} - m [D]}{RT}\right)} \quad (1)$$

$R_{H,N}$ and $R_{H,U}$ denote the hydrodynamic radius of the native and unfolded form of the peptide, respectively, T is absolute temperature in Kelvin and R is universal gas constant. ΔG^{H_2O} denotes the Gibbs free energy in the absence of denaturant and can be used to assess the structural stability of a peptide¹⁵. m is a measure of cooperativity of the unfolding transition and is proportional to the change in the solvent-accessible surface area ($\Delta SASA$) when going from the native to the denatured conformation¹⁶. This will be discussed in more detail in the Supplementary Information. The denaturant concentration is given by $[D]$. Equation (1) incorporates the linear extrapolation model which assumes a linear relationship between the Gibbs free energy ΔG and the denaturant concentration¹⁷:

$$\Delta G = \Delta G^{H_2O} - m [D] \quad (2)$$

For a better comparability between several independent measurement series, the hydrodynamic radii from the FCS unfolding experiments were also transformed into the fraction of denatured peptide f_{exp} by the following equation:

$$f_{\text{exp}} = \frac{R_H - R_{H,\text{min}}}{R_{H,\text{max}} - R_{H,\text{min}}} \quad (3)$$

$R_{H,\text{min}}$ and $R_{H,\text{max}}$ denote the smallest and largest measured hydrodynamic radius of the peptide, respectively. With the fractions of the native and unfolded form of the peptide, f_N and f_U , equation (1) turns to:

$$f = \frac{f_N + f_U \exp\left(-\frac{\Delta G^{H_2O} - m [D]}{RT}\right)}{1 + \exp\left(-\frac{\Delta G^{H_2O} - m [D]}{RT}\right)} \quad (4)$$

Results and Discussion

AF488-C(0)A β 42 is monomeric under FCS measuring conditions. Purely monomeric AF488-C(0)A β 42 was prepared from recombinant C(0)A β 42 after AF488 coupling to the cysteine residue and subsequent size exclusion chromatography (SEC) (Fig. S1 in the Supplementary Information). The time between SEC purification and the FCS unfolding measurements ranged from minutes to hours. We have not observed any dependence of the experimental results on the lag time between SEC purification and experiment start. There was no indication for the presence of AF488-C(0)A β 42 aggregates from FCS analysis (Figs 1 and S2).

Hence, in order to be sure that the unfolding transition is solely due to conformational changes of the monomers, we performed PCH analysis on the data set of the FCS unfolding experiments, particularly at the lowest GdnHCl concentration (0.25 M) and at a high GdnHCl concentration (5 M). In case there would have been oligomers present in the solution, a one-component fit to the experimental PCH would have failed and resulted in a reduced chi-squared much higher than one. Figure 2 reveals that fitting the experimental PCH of AF488-C(0)A β 42 with a one-component model yielded a good fit with a reduced chi-squared close to one over the entire GdnHCl concentration range.

In addition, the brightness values of free AF488 dye and AF488-C(0)A β 42 were almost identical at 0.25 M and 5 M GdnHCl, respectively (Table 1). A substantial amount of oligomeric species would have yielded a higher brightness of AF488-C(0)A β 42 compared to the free dye¹³. The 2.5–3-fold smaller brightness at 5 M GdnHCl results from a bathochromic shift in the excitation and emission spectra (Fig. S8), which leads to a decrease in the detected intensity since the excitation and emission filter set was chosen according to the non-shifted spectrum at zero molar GdnHCl. It shall be noted that the verification of the monomeric form was performed on the same

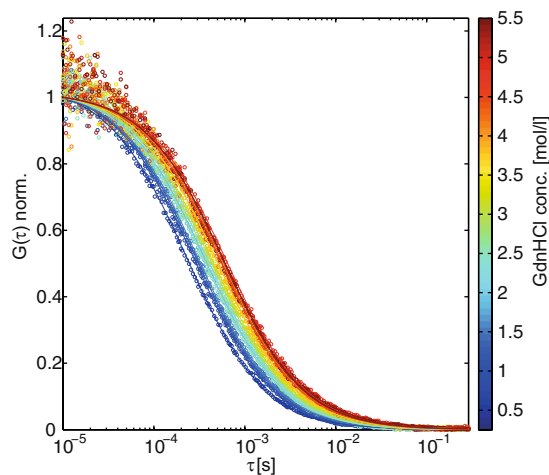


Figure 1. Normalized correlation curves (○) with their corresponding best-fit lines (—) of AF488-C(0)Aβ42 under denaturing conditions of increasing GdnHCl concentrations and based on a one-component diffusion model (equation (S1) in the Supplementary Information). The shift towards larger correlation times can mainly be attributed to (i) the increasing viscosity of the GdnHCl solutions and (ii) an increase of the hydrodynamic radius due to the unfolding process.

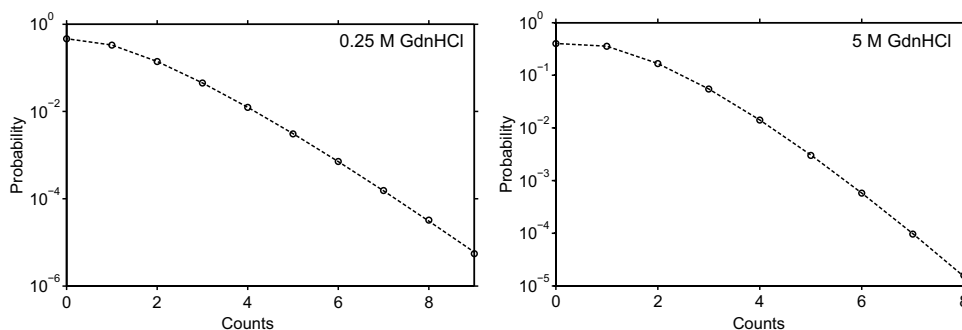


Figure 2. Photon counting histograms of AF488-C(0)Aβ42 in 0.25 M GdnHCl solution (left) and in 5 M GdnHCl solution (right). 0.25 M GdnHCl was the lowest GdnHCl concentration applied in the 1fFCS measurements whose data was used to generate the photon counting histograms. Each dashed line in this figure represents a fit to a one-component model. A reduced chi-squared of $\chi_r^2 = 0.6$ and 1.2, respectively, indicates an excellent fit to this model where the F-value (equation (S16)) was determined from a separate measurement with free AF488 dye.

sample	AF488		AF488-C(0)Aβ42	
GdnHCl conc. [M]	0.25	5	0.25	5
brightness [kHz]	16.23 (±0.22)	6.36 (±0.43)	18.73 (±2.23)	6.32 (±0.18)

Table 1. Comparison of the brightnesses of free AF488 dye and AF488-C(0)Aβ42 in 0.25 M and 5 M GdnHCl solution obtained from PCH analysis (Fig. 2).

data set, which was finally used to construct the unfolding curve. This is in contrast to other methods such as circular dichroism (CD) spectroscopy or 4,4'-bis-1-anilino-naphthalene-8-sulfonate (Bis-ANS) fluorescence in which the verification is done on a separate instrument (e.g. SEC) after the actual unfolding measurements (see e.g. ref. 18).

Monomeric AF488-C(0)Aβ42 shows a cooperative unfolding transition. Upon unfolding in GdnHCl, the increasing hydrodynamic radii, as well as the increasing viscosity of the solutions, leads to a right-shift of the correlation curves, as shown in Fig. 1. For quantifying the unfolding effect, the correlation curves were fitted by a one-component diffusion model (equation (S1)) and the corresponding diffusion coefficients were converted into hydrodynamic radii via the Stokes-Einstein relation. Plotting the hydrodynamic radii as a function of the GdnHCl concentration yields the appropriate unfolding curves shown in Fig. 3A and B.

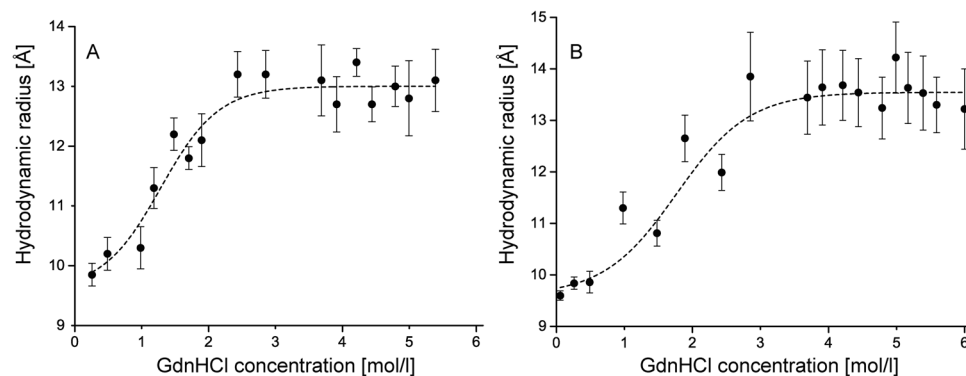


Figure 3. AF488-C(0)A β 42 unfolding curves as obtained by the analysis of a single 1fFCS measurement series (A) and as obtained by the analysis of a single 2fFCS measurement series (B). The dashed lines are best-fit lines to the two-state unfolding model (equation (1)). The hydrodynamic radius is plotted as a function of the GdnHCl concentration. The error bars of the unfolding curves were derived as the standard deviation of the fitting results of 10 correlation curves per data point.

method	ΔG^{H_2O} [kcal/mol]	m [kcal/mol/M]
1fFCS	2.6 (± 0.7)	1.7 (± 0.5)
2fFCS	1.9 (± 0.5)	1.1 (± 0.3)
average	2.3 (± 0.6)	1.4 (± 0.4)

Table 2. Fit parameter from fitting the unfolding curves (Fig. 3A and B) to the two-state unfolding model (equation (1)).

We measured a whole unfolding series of AF488-C(0)A β 42 using 2fFCS and compared the corresponding unfolding curve with one obtained by 1fFCS in order to validate that the 1fFCS results are not biased by refractive-index changes. Both unfolding curves show a similar course with a transition region between 1 and 2.5 M GdnHCl. The hydrodynamic radius $R_{H,N}$ at about zero molar GdnHCl corresponds to the hydrodynamic radius of the native conformation. The $R_{H,N}$ value is about 9.6 Å for both methods, which is in good agreement with the results reported in studies that characterized A β isoforms^{19–21}. The hydrodynamic radius of the unfolded conformation $R_{H,U}$ can be extracted from the unfolding curve at high GdnHCl concentrations (3 to 6M) and is about 13.0 Å (A) or 13.6 Å (B). Because A β 42 is small and believed to be unstructured to some extent the absolute change in hydrodynamic radius upon unfolding was expected to be much smaller than for other proteins^{22–24}. Our results confirm our assumption.

The steepness of the unfolding curve in the transition region contains information about the structural stability of the peptide. This information is enclosed in the m -value and ΔG^{H_2O} , respectively (equations (1) and (2)), whereas the latter one reports on the stability of the native conformation of a protein in the absence of denaturant¹⁵ and can thus, for example, be used to compare protein mutants with their corresponding wild-type²⁵. Both parameters can be extracted by fitting the experimental unfolding curve to a two-state unfolding model (equation (1)). As presented in Table 2, the parameters ΔG^{H_2O} and m are very close together.

It shall be mentioned that the 1fFCS and 2fFCS unfolding curves in Fig. 3A and B are based on a single measurement series each, which results in small error bars of the unfolding curves and correspondingly in small errors of the fit parameters. In this case, the error bars of the unfolding curves were derived as the standard deviation of the fitting results of 10 correlation curves per data point. Within one measurement series, the error bars tend to increase with increasing GdnHCl concentrations. The reasons for this may be manifold and are discussed in the Supplementary Information (Figs S3–S5 and S8). Furthermore, it was checked whether the change in hydrodynamic radius is associated with the unfolding of the A β 42 peptide and not to structural changes of the conjugated AF488 dye. For this purpose, the free AF488 dye was measured at several GdnHCl concentrations up to 6 M and no increase in hydrodynamic radius was observed (Fig. S6).

The experimental data was normalized by using equation (3). Consequently, the fraction of unfolded peptide is plotted as a function of the GdnHCl concentration, leading to the unfolding curve presented in Fig. 4. Figure 4 shows the unfolding curve of AF488-C(0)A β 42 from three independent 1fFCS and one 2fFCS measurement series. The hydrodynamic radii of the folded and the unfolded states are fully reproducible at around 9.6 and 13 Å, respectively, but the hydrodynamic radii around the transition points showed larger variations between independent measurement series. Thus, although each single unfolding curve is within the error margins of the other unfolding curves, the combined unfolding curve results in error bars that are larger around the transition point than at low and high GdnHCl concentrations. Therefore, the error bars of the corresponding fit parameters in Table 3, which are in line with the values calculated in Table 2, are also larger. AF488-C(0)A β 42 is predominantly in its native conformation up to 0.5 M GdnHCl. A relatively steep transition region between 1 and 2 M GdnHCl is followed by a plateau above 2 M at which the AF488-C(0)A β 42 was completely unfolded. Each data point was

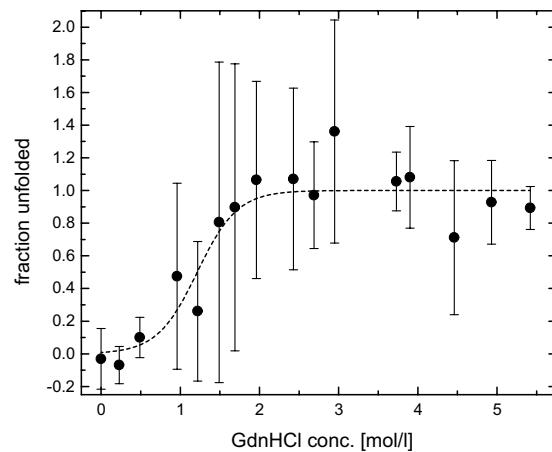


Figure 4. Unfolding curve of AF488-C(0)A β 42 from three independent 1fFCS and one 2fFCS measurement series with their corresponding best-fit line to the two-state unfolding model (equation (4)). Each data point is the average of at least three hydrodynamic radii, which were transformed into the fraction of denatured peptide according to equation (3). The error bars were calculated as the standard deviation between these independent measurements.

ΔG^{H_2O} [kcal/mol]	m [kcal/mol/M]
2.8 (\pm 1.2)	2.3 (\pm 0.9)

Table 3. Fit parameters from fitting the unfolding curve (Fig. 4) to the linear extrapolation model (equation (3)). The fit was performed on the averaged unfolding curve. The errors denote the standard errors of the fit parameters.

measured at least in triplicate. Thus, the corresponding error bars in Fig. 4 were calculated as the standard deviation between these independent measurements.

The ΔG^{H_2O} -value calculated in Table 3 is reasonably low and indicates that, from a thermodynamic point of view, there is energetically no considerable difference between the unfolded conformation and the native conformation (free in solution). Depending on the free energy of activation for the interconversion of both conformations, the equilibrium will quickly be achieved once the AF488-C(0)A β 42 is formed in its native conformation. Buell *et al.* showed that the Gibbs free energy of activation for the conformational change of native A β 42 to a beta-sheet conformation (as found in fibrils) is very low (1.4 kcal/mol)²⁶. If we assume a similar value for the interconversion between the native and the unfolded state, chemical equilibrium will be reached quickly. In addition, it was shown that a low ΔG^{H_2O} -value corresponds to a high aggregation propensity²⁷, which goes well with the known properties of A β 42²⁸.

It is worth mentioning that our ΔG^{H_2O} -value is larger than typical values for the strength of hydrogen bonds within proteins (\approx 0.5–1.5 kcal/mol²⁹). Hence, the native conformation might contain several hydrogen bonds which leads to some residual structure, *e.g.* a short beta-sheet at the C-terminus²⁸ or a molten globule in which the overall structure is denatured with some residual structural elements³⁰. In a molten globule many hydrophobic residues can be surface-exposed and lead to a sticky behaviour of the corresponding peptide, which also goes well with the properties of A β 42^{31,32}. In any case, the results do not agree with a completely randomly coiled peptide as opposed to what is partially claimed in the literature^{33,34}.

Our results show a cooperative unfolding of monomeric AF488-C(0)A β 42 with a Gibbs free energy of about 2.8 kcal/mol. The peptide contains some residual structural elements and is thus not completely random coiled. We think that monomeric A β 42 adopts a molten globule conformation under physiological conditions. A future study is going to examine this issue, which is, however, beyond the scope of this paper.

Conclusions

With this study, we explored the unfolding of dye-labelled monomeric amyloid- β 42 (A β 42) peptide under near-physiological conditions using fluorescence correlation spectroscopy. We showed that this technique is able to track the tiny changes of the hydrodynamic radius when monomeric A β 42 unfolds in guanidine hydrochloride. We found that A β 42 shows a cooperative unfolding, which clearly suggests the presence of structural elements. However, the small value of the Gibbs free energy of unfolding (\approx 2.8 kcal/mol) indicates that only a low amount of residual structure is present and that A β 42 is mainly unfolded. Our results hint that monomeric A β 42 adopts a molten globule conformation.

References

- Crescenzi, O. *et al.* Solution structure of the Alzheimer amyloid beta-peptide (1–42) in an apolar microenvironment. *Eur. J. Biochem.* **269**, 5642–5648, doi:10.1046/j.1432-1033.2002.03271.x (2002).
- Tomaselli, S. *et al.* The alpha-to-beta conformational transition of Alzheimer's Aβ(1–42) peptide in aqueous media is reversible: a step by step conformational analysis suggests the location of beta conformation seeding. *ChemBioChem* **7**, 257–267, doi:10.1002/cbic.v7:2 (2006).
- Seubert, P. *et al.* Isolation and quantification of soluble Alzheimer's beta-peptide from biological fluids. *Nature* **359**, 325–327, doi:10.1038/359325a0 (1992).
- Lazo, N. D., Grant, M. A., Condrón, M. C., Rigby, A. C. & Teplow, D. B. On the nucleation of amyloid beta-protein monomer folding. *Protein Sci.* **14**, 1581–1596, doi:10.1110/ps.041292205 (2005).
- Lührs, T. *et al.* 3D structure of Alzheimer's amyloid-β(1–42) fibrils. *PNAS* **102**, 17342–17347, doi:10.1073/pnas.0506723102 (2005).
- Frost, D., Gorman, P. M., Yip, C. M. & Chakrabarty, A. Co-incorporation of Aβ40 and Aβ42 to form mixed pre-fibrillar aggregates. *FEBS J.* **270**, 654–663, doi:10.1046/j.1432-1033.2003.03415.x (2003).
- Nozaki, Y. The preparation of guanidine hydrochloride. *Methods Enzymol.* **26**, 43–50, doi:10.1016/S0076-6879(72)26005-0 (1972).
- Enderlein, J. & Gregor, I. Using fluorescence lifetime for discriminating detector afterpulsing in fluorescence-correlation spectroscopy. *Rev. Sci. Instrum.* **76**, 033102, doi:10.1063/1.1863399 (2005).
- Dertinger, T. *et al.* Two-focus fluorescence correlation spectroscopy: a new tool for accurate and absolute diffusion measurements. *Chemphyschem* **8**, 433–443, doi:10.1002/cphc.200600638 (2007).
- Müller, C. & Richtering, W. Sealed and temperature-controlled sample cell for inverted and confocal microscopes and fluorescence correlation spectroscopy. *Colloid Polym Sci* **286**, 1215–1222, doi:10.1007/s00396-008-1901-3 (2008).
- Müller, J. D., Chen, Y. & Gratton, E. Resolving heterogeneity on the single molecular level with the photon-counting histogram. *Biophys. J.* **78**, 474–486, doi:10.1016/S0006-3495(00)76610-0 (2000).
- Meseth, U., Wohland, T., Rigler, R. & Vogel, H. Resolution of fluorescence correlation measurements. *Biophys. J.* **76**, 1619–1631, doi:10.1016/S0006-3495(99)77321-2 (1999).
- Chen, Y., Wei, L.-N. & Müller, J. D. Probing protein oligomerization in living cells with fluorescence fluctuation spectroscopy. *PNAS* **100**, 15492–15497, doi:10.1073/pnas.2533045100 (2003).
- Chen, Y., Müller, J. D., So, P. T. & Gratton, E. The photon counting histogram in fluorescence fluctuation spectroscopy. *Biophys. J.* **77**, 553–567, doi:10.1016/S0006-3495(99)76912-2 (1999).
- Pace, C. N. The stability of globular proteins. *CRC Crit. Rev. Biochem.* **3**, 1–43, doi:10.3109/10409237509102551 (1975).
- Myers, J. K., Pace, C. N. & Scholtz, J. M. Denaturant m values and heat capacity changes: relation to changes in accessible surface areas of protein unfolding. *Protein Sci.* **4**, 2138–2148, doi:10.1002/pro.v4:10 (1995).
- Pace, C. N. & Shaw, K. L. Linear extrapolation method of analyzing solvent denaturation curves. *Proteins (Suppl 4)*, 1–7 (2000).
- Barrow, C. J., Yasuda, A., Kenny, P. T. & Zagorski, M. G. Solution conformations and aggregational properties of synthetic amyloid beta-peptides of Alzheimer's disease. *J. Mol. Biol.* **225**, 1075–1093, doi:10.1016/0022-2836(92)90106-T (1992).
- Nag, S. *et al.* Nature of the Amyloid-β Monomer and the Monomer-Oligomer Equilibrium. *J. Biol. Chem.* **286**, 13827–13833, doi:10.1074/jbc.M110.199885 (2011).
- Bitan, G. *et al.* Amyloid-β-protein (Aβ) assembly: Aβ40 and Aβ42 oligomerize through distinct pathways. *PNAS* **100**, 330–335, doi:10.1073/pnas.222681699 (2003).
- Mittag, J. J., Milani, S., Walsh, D. M., Rädler, J. O. & McManus, J. J. Simultaneous measurement of a range of particle sizes during Aβ_{1–42} fibrillogenesis quantified using fluorescence correlation spectroscopy. *Biochem. Biophys. Res. Com.* **448**, 195–199, doi:10.1016/j.bbrc.2014.04.088 (2014).
- Sasmal, D. K. *et al.* An FCS study of unfolding and refolding of CPM-labeled human serum albumin: role of ionic liquid. *J. Phys. Chem. B* **115**, 13075–13083, doi:10.1021/jp207829y (2011).
- Sherman, E. *et al.* Using fluorescence correlation spectroscopy to study conformational changes in denatured proteins. *Biophys. J.* **94**, 4819–4827, doi:10.1529/biophysj.107.120220 (2008).
- Chattopadhyay, K., Saffarian, S., Elson, E. L. & Frieden, C. Measuring unfolding of proteins in the presence of denaturant using fluorescence correlation spectroscopy. *Biophys. J.* **88**, 1413–1422, doi:10.1529/biophysj.104.053199 (2005).
- Pace, C. N., Shirley, B. A. & Thomson, J. A. Measuring the conformational stability of a protein In *Protein Structure: a practical approach* (ed. Creighton, T.E.) 311–330 (IRL Press, Oxford, 1989).
- Buell, A. K. *et al.* Detailed analysis of the energy barriers for amyloid fibril growth. *Angew. Chem. Int. Ed.* **51**, 5247–5251, doi:10.1002/anie.201108040 (2012).
- Ni, C.-L., Shi, H.-P., Yu, H.-M., Chang, Y.-C. & Chen, Y.-R. Folding stability of amyloid-beta 40 monomer is an important determinant of the nucleation kinetics in fibrillization. *FASEB J.* **25**, 1390–1401, doi:10.1096/fj.10-175539 (2011).
- Sgourakis, N. G., Yan, Y., McCallum, S., Wang, C. & Garcia, A. E. The Alzheimer's peptides Aβ40 and 42 adopt distinct conformations in water: a combined MD/NMR study. *J. Mol. Biol.* **368**, 1448–1457, doi:10.1016/j.jmb.2007.02.093 (2007).
- Sheu, S.-Y., Yang, D.-Y., Selzle, H. L. & Schlag, E. W. Energetics of hydrogen bonds in peptides. *PNAS* **100**, 12683–12687, doi:10.1073/pnas.2133366100 (2003).
- Enderlein, J. Collapsed but not folded: looking with advanced optical spectroscopy at protein folding. *Chemphyschem* **8**, 1607–1609, doi:10.1002/cphc.200700247 (2007).
- Ahyayauch, H. *et al.* Binding of β-amyloid (1–42) peptide to negatively charged phospholipid membranes in the liquid-ordered state: modeling and experimental studies. *Biophys. J.* **103**, 453–463, doi:10.1016/j.bpj.2012.06.043 (2012).
- Bateman, D.A., McLaurin, J. & Chakrabarty, A. Requirement of aggregation propensity of Alzheimer amyloid peptides for neuronal cell surface binding. *BMC Neuroscience* **8** (2007).
- Tran, L., Basdevant, N., Prévost, C. & Ha-Duong, T. Structure of ring-shaped Aβ₄₂ oligomers determined by conformational selection. *Sci. Rep.* **6**, 21429, doi:10.1038/srep21429 (2016).
- Shao, H., Jao, S., Ma, K. & Zagorski, M. G. Solution Structures of Micelle-bound Amyloid β-(1–40) and β-(1–42) Peptides of Alzheimer's Disease. *J. Mol. Biol.* **285**, 755–773, doi:10.1006/jmbi.1998.2348 (1999).

Acknowledgements

We are grateful to Stefan Klinker and Lothar Gremer for their help with the amyloid-β expression and purification and for their C(0)Aβ42 gift. We thank Filipp Oesterhelt for providing the 1fFCS/FFS setup. M.S. thanks the graduate school iGRASP seed and the NRW Research School BioStruct for funding.

Author Contributions

M.S. designed the experiments. M.S., S.W. and C.C. performed the experiments. M.S. and S.W. analysed the data. M.S., S.W., W.R. and D.W. wrote the manuscript. M.S. and S.W. contributed equally to this work.

Additional Information

Supplementary information accompanies this paper at doi:[10.1038/s41598-017-02410-y](https://doi.org/10.1038/s41598-017-02410-y)

Competing Interests: The authors declare that they have no competing interests.

Publisher's note: Springer Nature remains neutral with regard to jurisdictional claims in published maps and institutional affiliations.



Open Access This article is licensed under a Creative Commons Attribution 4.0 International License, which permits use, sharing, adaptation, distribution and reproduction in any medium or format, as long as you give appropriate credit to the original author(s) and the source, provide a link to the Creative Commons license, and indicate if changes were made. The images or other third party material in this article are included in the article's Creative Commons license, unless indicated otherwise in a credit line to the material. If material is not included in the article's Creative Commons license and your intended use is not permitted by statutory regulation or exceeds the permitted use, you will need to obtain permission directly from the copyright holder. To view a copy of this license, visit <http://creativecommons.org/licenses/by/4.0/>.

© The Author(s) 2017